Domain compliance and elastic power transmission in rotary F_OF_1-ATPase

Hendrik Sielaff[a], Henning Rennekamp[a], André Wächter[a,b], Hao Xie[a], Florian Hilbers[a], Katrin Feldbauer[a,1], Stanley D. Dunn[c], Siegfried Engelbrecht[a,b], and Wolfgang Junge[a,2]

Departments of [a]Biophysics and [b]Biochemistry, University of Osnabrück, 49069 Osnabrück, Germany; and [c]Department of Biochemistry, University of Western Ontario, London, ON, Canada N6A 5C1

Edited by Hartmut Michel, Max Planck Institute for Biophysics, Frankfurt, Germany, and approved October 3, 2008 (received for review August 5, 2008)

The 2 nanomotors of rotary ATP synthase, ionmotive F_O and chemically active F_1, are mechanically coupled by a central rotor and an eccentric bearing. Both motors rotate, with 3 steps in F_1 and 10–15 in F_O. Simulation by statistical mechanics has revealed that an elastic power transmission is required for a high rate of coupled turnover. Here, we investigate the distribution in the F_OF_1 structure of compliant and stiff domains. The compliance of certain domains was restricted by engineered disulfide bridges between rotor and stator, and the torsional stiffness (κ) of unrestricted domains was determined by analyzing their thermal rotary fluctuations. A fluorescent magnetic bead was attached to single molecules of F_1 and a fluorescent actin filament to F_OF_1, respectively. They served to probe first the functional rotation and, after formation of the given disulfide bridge, the stochastic rotational motion. Most parts of the enzyme, in particular the central shaft in F_1, and the long eccentric bearing were rather stiff (torsional stiffness κ > 750 pNnm). One domain of the rotor, namely where the globular portions of subunits γ and ε of F_1 contact the c-ring of F_O, was more compliant ($\kappa \cong 68$ pNnm). This elastic buffer smoothes the cooperation of the 2 stepping motors. It is located were needed, between the 2 sites where the power strokes in F_O and F_1 are generated and consumed.

elasticity | F-ATPase | nanomotor

Molecular motors abound in the cell. It is worth asking whether or not a discrete power stroke, usually caused by the hydrolysis of ATP or the transport of an ion, is fine-tuned to the detailed molecular events that are powered by the respective motor. In ATP synthase (F_OF_1-ATPase), for instance, the rotary electromotor, F_O, drives the rotary chemical generator, F_1, to synthesize ATP. Whereas F_O, depending on the organism, processes in 10–15 steps per turn, F_1 processes in 3 steps. As an alternative to the fine-tuning of the underlying partial reactions, it has been proposed (refs. 1–4 and references therein) that an elastic power transmission might serve to smooth the coupled operation of the counteracting rotary motors. To substantiate this claim here, we determined the distribution of stiff and compliant domains over the molecular structure of this enzyme.

The ATP synthase from *Escherichia coli*, EF_OF_1, is composed of 8 different subunits attributable either to the "rotor," namely, subunits γ and ε of F_1 plus the c_{10} ring of F_O (5), or to the "stator," namely, subunits δ and $(\alpha\beta)_3$ of F_1 plus subunits a and b_2 of F_O. The rotor portion of F_1 is linked to the rotor portion of the ion-motive F_O by interfacing subunits γ and ε of F_1 with the c-ring of F_O. The crystal structure of the bovine mitochondrial F_1 (MF_1) (6) has revealed the threefold pseudosymmetry of the hexagon formed by subunits α and β, which are arranged as $(\alpha\beta)_3$. Under ATP hydrolysis, the structural symmetry of 3 is paralleled by the rotation of the γ subunit in 3 steps of 120° with substeps of 40° and 80° (7–9). The c-ring ion-driven motor, F_O, contains 10–15 identical monomers, depending on the organism and, supposedly, steps by 24°–36°. The symmetry does match in some organisms (3:15) but not in others (e.g., 3:14 in chloroplast CF_OF_1 and 3:10 in yeast and *E. coli*) (see refs.10–12 and references therein).

First evidence for an elastic coupling element in F_OF_1 has been provided by simulations of its kinetic properties both under rate limitation by proton transfer in F_O (13) and by catalysis in F_1 (14). A first estimate for the torsional stiffness of the elastic element in EF_OF_1 has been obtained from recordings of the torque as a function of the angular reaction coordinate (4). A single molecule of F_OF_1 has been immobilized with F_1 down on a solid support with a fluorescent actin filament attached to the c-ring of F_O to monitor the rotation as driven by the hydrolysis of ATP. Because of the viscous drag on the long filament (length >3 μm) the turnover rate is reduced by >2 orders of magnitude compared with the rate without filament. The viscous drag counteracts the enzyme-generated torque, and this bends the filament. As with a spring balance, its curvature was used to determine the torque as a function of the angular position of the c-ring. Although the driving motor, F_1, progressed in steps (of 120°), the torque profile, as sensed by F_O, was smooth, and this was attributed to an elastic coupling element with a torsional stiffness of ≈60 pNnm (4). The theoretical treatment of this nanomachine in terms of the Smoluchowski equation of statistical mechanics has revealed the benefit of an elastic buffer, which is required for a high turnover rate under load (see figure 8 in ref. 4 and also ref. 15). Although the existence of an elastic power transmission between F_O and F_1 has been established by the above-cited work (4), the magnitude and the distribution of compliant versus stiff elements over the enzyme structure, in particular between central rotor and eccentric stator, has not been determined before. Here, we investigated the torsional stiffness of several enzyme domains by fluctuation analysis, and localized the elastic buffer in the structure of EF_OF_1. The domain compliance was investigated by monitoring either via a magnetic bead (diameter typically 1 μm) or by a short actin filament (length <0.5 μm) the thermal rotational fluctuations of an attached fluorescent probe in immobilized single molecules. To attribute the observed overall compliance to specific enzyme domains we stiffened selected portions by disulfide cross-linking through engineered cysteines. The properties of the respective cysteine pairs, their position in the crystal structure and the correlation between the functional halt positions of the active enzyme, the disulfide-locked conformations, and the published crystal structures have been presented elsewhere (46).

Author contributions: H.S. and W.J. designed research; H.S., H.R., A.W., H.X., F.H., and K.F. performed research; H.S., S.D.D., and S.E. contributed new reagents/analytic tools; H.S., H.R., A.W., H.X., F.H., K.F., S.E., and W.J. analyzed data; and H.S., A.W., S.D.D., S.E., and W.J. wrote the paper.

The authors declare no conflict of interest.

This article is a PNAS Direct Submission.

[1]Present address: Max Planck Institute for Biophysics, 60438 Frankfurt, Germany.

[2]To whom correspondence should be addressed at: Universität Osnabrück, FB Biologie/Chemie, R.35/42, Barbarastrasse 11, D-49076 Osnabrück, Germany. E-mail: junge@uos.de.

This article contains supporting information online at www.pnas.org/cgi/content/full/0807683105/DCSupplemental.

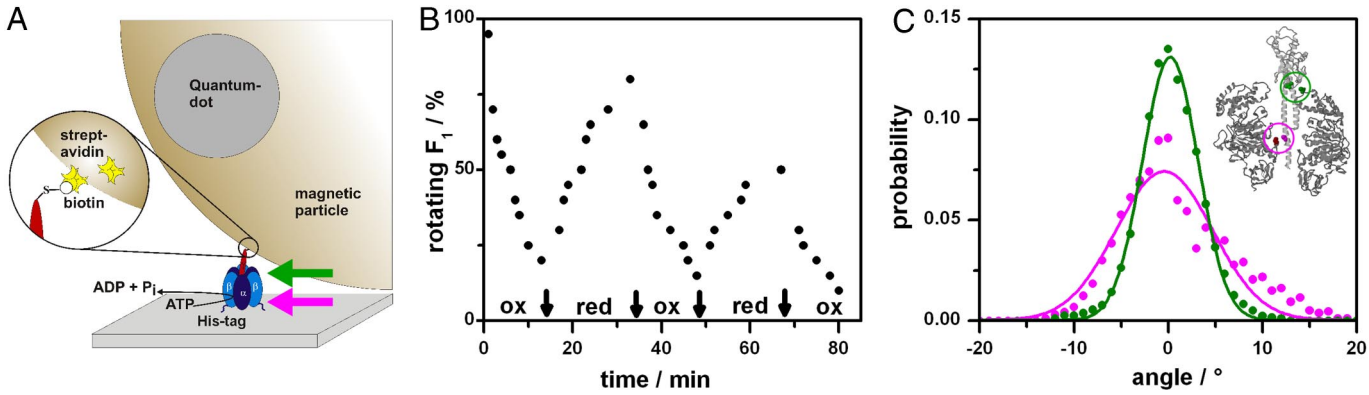

Fig. 1. Immobilized EF_1 with attached magnetic bead (*A*), the yield of magnetically forced rotation as function of oxidation-reduction cycles (*B*), and histograms of thermally driven rotational fluctuations (magnetic field off) after the formation of a disulfide cross-link between the rotor and the stator (*C*). The green and magenta arrows in *A* indicate the position of the particular disulfide cross-links in EF_1. They are encircled in green and magenta, respectively, in *C* Inset. The arrows in *B* indicate the time when the solution was changed from reducing to oxidizing and vice versa. The points in *C* are experimental, and the lines are the respective fits by a single Gaussian. For details, see *Results*.

Results

Magnetically Driven Rotation and Rotational Fluctuations in EF_1. Magnetically driven rotation and rotational fluctuations in EF_1 were studied as follows. A single molecule of EF_1 was immobilized on a Ni-NTA-coated glass plate by an engineered His-tag at the N-terminal end of each of the three copies of subunit β as illustrated in Fig. 1A. A streptavidin-coated hyperparamagnetic bead was attached with a biotin-maleimide function to the rotor via an engineered cysteine in the bulky protruding domain of subunit γ (γK109C). The bead, typical diameter 1 μm, was fluorescence-labeled by biotinylated quantum-dots (Q-dots), allowing for extended observation times without bleaching. A slowly rotating magnetic field (typically 0.1 revolutions per second) was applied (5 mM Mg-ATP present), and the orientation of the bead was videographed in an inverted fluorescence microscope. If the viewing field contained, say 100 beads total, it typically showed 95 rotating ones. Whether or not this was a relevant, enzyme-related rotation was checked as follows. Aside from the above-mentioned cysteine serving to attach the bead, the mutant EF_1 contained 2 additional cysteines; they were engineered to form a zero-length cross-link between rotor and stator under oxidizing conditions, placed opposite each other in the homology structure of EF_1 to the crystal structure of MF_1 (6). The location of 2 cysteine pairs in the enzyme structure is indicated in Fig. 1*C*. The magnetically driven rotation of the beads stopped after perfusion of the reaction chamber with an oxidant while the rotating field was still on. Fig. 1*B* shows the percentage of rotating over total beads in the viewing field as function of 3 cycles where the solution over the glass plate was changed from reducing to oxidizing and back. The loss of rotating beads from 1 redox cycle to the other was due to the detachment of beads/enzymes from the solid support by the shear flow during exchange of solution. It was obvious from Fig. 1*B* that (*i*) the formation and cleavage of the disulfide bonds was reversible and (*ii*) that the rotation of the great majority of beads was related to the rotation of subunit γ in the $(\alpha\beta)_3$-corpus of EF_1. In other words, the data excluded that the bead/EF_1-construct rotated as a whole (e.g., around 1 His-tag), that beads were dancing around their attachment sites on EF_1, or, unattached to F_1, around an unspecific attachment site on the glass surface.

Keeping 1 particular rotating bead in focus, its enzyme molecule was locked by changing the solution from reducing to oxidizing. Then the magnetic field was switched off. As a consequence, the bead only showed rotary thermal fluctuations of rather narrow width. The probability distribution of these fluctuations was determined and fitted by a single Gaussian. Two such histograms are shown in Fig. 1*C*. The distribution was wider for the double mutant αE284C/γA270C (in magenta) than for the double mutant βD380C/γA87C (in green). Good reproducibility of this width from 1 single molecule of a given mutant enzyme to the other [see supporting information (SI) Fig. S1] showed that the different widths between these 2 mutants was meaningful.

One might ask whether the rotational fluctuation of the large bead, its diameter being by 2 orders of magnitude greater than the one of the enzyme, are restricted by the enzyme's compliance or rather by surface contacts. Three lines of evidence showed that the fluctuation of the bead was related to the enzyme and was thus relevant: (*i*) The width of the thermal fluctuations was reproducible (see Fig. S1), and related to the position in the enzyme of the respective disulfide bridge (see Fig. 1*C*); (*ii*) only occasionally, we observed beads that were stuck at the surface, and this was immediately evident from a much narrower width of their fluctuations, typical full width at half maximum (FWHM) $<3°$, as compared with $>7°$ in the great majority of cases (see Fig. S2); (*iii*) in our related study on the orientation of the rotor during functional halts in comparison with its orientation as revealed by X-ray crystallography of the inhibited enzyme (46), we found that the difference between the "enzyme-intrinsic" stop-orientations, e.g., after ADP saturation, and after oxidation of an engineered cysteine pair (engineered stop) strictly depended on the position of the particular cysteine on the helical wheel of subunit γ (see Fig. S3). It excluded that these stop positions were dominated by surface contacts.

Rotary Fluctuations and the Torsional Stiffness. When a homogeneous, isotropic elastic rod is fixed at 1 end, whereas it is free at the other end, the thermal impact on the rod (the Langevin force) generates a fluctuating torque, M. It torsionally strains the free surface by an angle ϕ (in radians), such that $M = \kappa \cdot \phi$. The torsional stiffness of the rod, κ, is expressed in units of pNnm. The elastic energy that is transiently stored in the rod is $U = 1/2 \cdot \kappa \cdot \phi^2$, and the probability, $p(\phi)$, of finding a given deformation angle is given by Boltzmann's equation

$$p(\phi) = \text{const} \cdot \exp\left(-\frac{U}{k_B T}\right) = (2\pi \cdot \sigma^2)^{-\frac{1}{2}} \cdot \exp\left(-\frac{\phi^2}{2\sigma^2}\right), \qquad [1]$$

yielding a Gaussian whose variance, σ^2, reads:

$$\sigma^2 = k_B T \cdot \kappa^{-1}. \qquad [2]$$

If the elastic element is composed of 2 rods of different stiffnesses, κ_1 and κ_2, the resulting variance is the sum of the 2 reciprocal stiffnesses, again calibrated in terms of Boltzmann's constant $k_B T$.

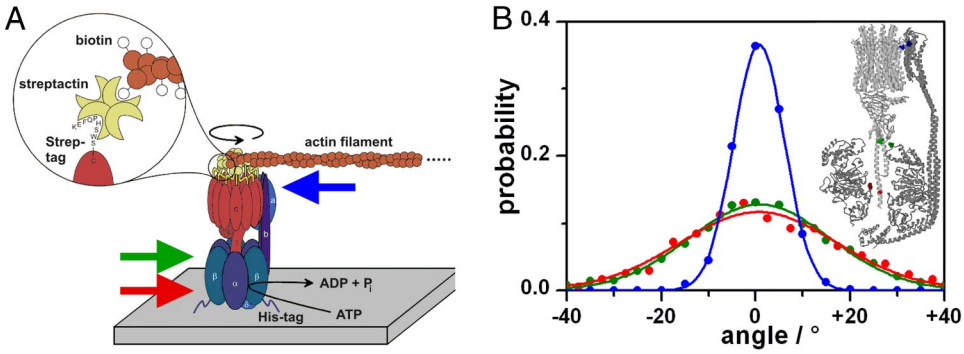

Fig. 2. Immobilized EF_OF_1 with attached actin filament of short length, typically 0.5 μm (*A*), and histograms of thermally driven rotational fluctuations after the formation of a disulfide cross-link between the rotor and the stator (*B*). The positions of 3 different disulfide cross-links are indicated in colors in *A* and in the *Inset* in *B*, with matching colors of the respective histograms. For details, see *Results*.

$$\sigma^2_{\text{comp}} = k_BT\cdot(\kappa_1^{-1} + \kappa_2^{-1}) = k_BT\cdot\kappa^{-1}_{\text{result}}. \quad [3]$$

If, instead of the standard deviation, σ, in radians, the FWHM of the distribution in degrees is read out, the stiffness, κ, reads as follows:

$$\kappa = 8\cdot\ln 2\cdot\left(\frac{180}{\pi}\right)^2\cdot k_BT\cdot(\text{FWHM})^{-2} \cong 73{,}700\ \text{pNnm}\cdot(\text{FWHM})^{-2}. \quad [4]$$

In summary: (*i*) The width of rotational fluctuations yields the torsional stiffness calibrated in terms of k_BT. (*ii*) In composite rods, the reciprocal stiffnesses are additive. (*iii*) The most compliant element stores the major portion of the elastic deformation energy, and it contributes most to the deformation angle.

Torsional Compliance of the Rotor Portion in EF_1. The evaluation of the original data shown in Fig. 1*C* according to Eq. **2** yielded a stiffness of ≈1,500 pNnm for the mutant βD380C/γA87C, where the disulfide link was placed close to the bead (green) and 500 pNnm for the mutant αE284C/γA270C (magenta), where it was farther down. The greater figure in the former mutant comprised compliance from all elements of the surface-to-enzyme-to-bead construct, in particular the rotational compliance of the His tags, and of the bead's attachment to the central shaft. All these "background compliances" were small, and the enzyme body and its attachment to the surface were stiff. The great stiffness was partially relieved in the mutant where the rotor/stator lock was placed farther down toward the C terminus of subunit γ (Fig. 1*C*, magenta). The increase of the compliance was thus attributable to the portion of subunit γ lying between the 2 sites chosen for blocking the rotation. We calculated a stiffness of κ = 750 pNnm for the particular portion of the central stalk lying between the green- and magenta-encircled sites as shown in Fig. 1*C*.

Torsional Compliance of the Rotor Portion in the Holoenzyme EF_OF_1. The torsional compliance of the rotor-portion in the holoenzyme, EF_OF_1, was determined by a similar procedure as for EF_1 except for 2 modifications, (*i*) ATP-driven (0.05–5 mM Mg-ATP) instead of magnetically driven rotation served to select relevant single molecules, and (*ii*) a fluorescent actin filament attached to the **c**-ring of F_O served as a probe. This construct is illustrated in Fig. 2*A*. Detergent-solubilized EF_oF_1 was immobilized by His tags. A fluorescent actin filament was attached to EF_o-$\mathbf{c}_{10}$ by biotin/streptactin linkage to engineered Strep-tags at the C termini of EF_o-**c** (16). The rotation of the $\mathbf{c}_{10}$-ring, driven by ATP hydrolysis, was recorded by microvideography. Short filaments (typically 0.5 μm) were used to avoid viscous overdamping of the stepped rotation (4, 17). Oxidizing conditions promoted the formation of a disulfide bridge between appropriately engineered cysteines on the stator and the rotor (see Fig. 2*B*), and this blocked the rotation.

Keeping a given rotating enzyme molecule in focus and changing the solution from reducing to oxidizing stopped the rotation. The rotational fluctuations persisted and were attributable to fluctuations within the enzyme. The actin filament itself contributed negligibly because of its short length (see ref. 17).

The *Inset* in Fig. 2*B* shows the location of the disulfide bridge in 3 mutants, namely (*i*) **a**I223C**c**L72C (blue), (*ii*) βD380C γA87C (green), and (*iii*) αE284CγA276C (red). The probability distributions of the respective rotational fluctuations are shown in matching colors in Fig. 2*B*. The respective FWHM translated into the following figures for the torsional stiffness in pNnm: (*i*) 450 (blue), (*ii*) 59 (green), and (*iii*) 47 (red). It implied a stiffness of <68 pNnm for the rotor segment lying between the blue and the green disulfide bridges. The stiffness of the segment between the green and the red disulfide bridges was not to be determined precisely here because of the great compliance of the segment farther up toward F_O.

The largest stiffness resulted if the **c**-ring was locked to subunit **a** (blue in Fig. 2*B*). The stiffening effect of this particular cross-link showed that the respective detergent-solubilized and surface-attached EF_OF_1 construct was intact and, in particular, that the attachment of the stator to the rotor was present. This qualifies the previous notion of a dangling stator in this EF_OF_1 construct (18). The smaller stiffness (450 pNnm) compared with the one observed with magnetic beads for F_1 (1,500 pNnm) was attributable to the compliance of the **c**-ring/F-actin construct. It was not caused by the attachment of F_1 to the solid support (see data in Fig. 1*C*).

Torsional Compliance of the Unrestricted, Active Enzyme. The torsional compliance of the unrestricted, active enzyme, e.g., during 1 ATP-waiting dwell before jumping by 120° into the next dwell, was inferred from long trajectories of rotation. Fig. 3*A* shows a short segment of a stepped rotary trajectory of 2-s duration, and Fig. 3*B* shows the respective angular probability distribution. The stiffness of the ADP-saturated and thereby intrinsically locked state (orange in Fig. 3*B*) was 66 pNnm, very much the same as when the DELSEED lever was cross-linked with the rotor (68 pNnm, green data in Fig. 2*B*). During the ATP-waiting dwells (typically of 100-ms duration, blue in Fig. 3*B*) the stiffness was κ = 30 pNnm. It implied that the lever motion (occurring during the ATP wait) contributed a stiffness of 50 pNnm.

Torsional Compliance of the Eccentric Bearing. The torsional compliance of the eccentric bearing was investigated in a construct illustrated in Fig. 4*A*. A cysteine was added to the C terminus of subunit **b** (bold letters in **NCM**NLN. . .). Two cysteines, one on each copy of the more or less parallel helices of subunit **b** (19–21), served as attachment sites for a Q-dot-doped magnetic bead via the maleimide–biotin link. Fig. 4*B* shows the probability distribution of the bead without magnetic field (*Upper*) and with the magnetic field turning steadily at 0.125 revolutions per second either clockwise (blue) or counterclockwise (red) when viewed from the F_O side (*Lower*). The sign of the displacement was chosen positive when moving in the counterclockwise direction. As expected, the rota-

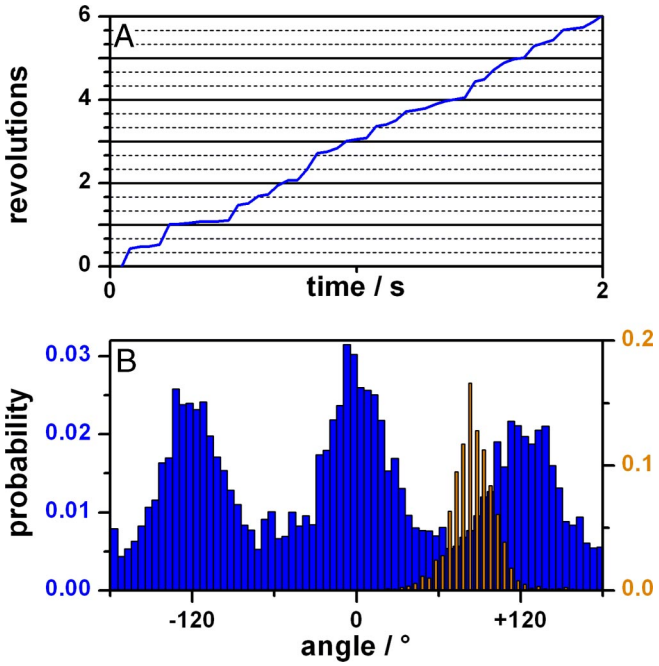

Fig. 3. Rotary trajectory under hydrolysis of ATP by active EF_OF_1 (*A*) and histogram of a more extended trajectory (*B*). The trajectory was recorded at 50 μM ATP with 5 mM Mg^{2+} present. As discussed in ref. 46, the halt positions represent the ATP-waiting dwells that follow each other with a period of 120°. The duration of these dwells, some 100 ms, was typical for immobilized EF_OF_1. The waiting for ATP binding was not diffusion-controlled. The orange histogram represents fluctuations after the molecule has fallen into its ADP-saturated state. Its peak was always displaced by −40° relative to the nearest one of the 3 ATP-waiting dwells. Details of the relation between the stepping motion and the crystal structure have been published in ref. 46.

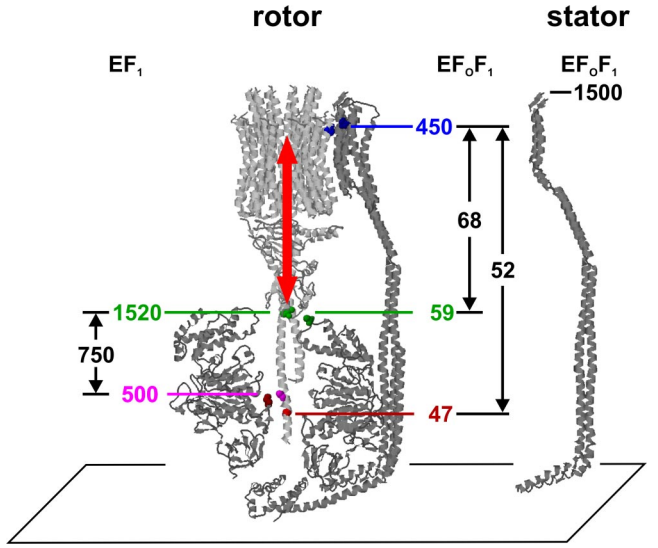

Fig. 5. Structural model of EF_OF_1 (stator subunits in dark gray, rotor in light gray) and, at the very right side, of the homodimer of subunit b, and numbers for the torsional stiffness of various domains. Numbers given on the left side resulted from data obtained with EF_1 in the setup shown in Fig. 1*A*, those on the right side from EF_OF_1 as in Fig. 2*A*, and the one at the far right from EF_OF_1 as in Fig. 4*A*. The stiffness κ comes in units of pNnm. Numbers associated with horizontal colored lines denote the resulting stiffness κ_{result} (see Eq. **3**) as observed when the respective disulfide cross-link (its 2 cysteines shown in the same hue, dark on the stator or light on the rotor) was closed. The numbers between the black vertical arrows denote the stiffnesses of the rotor domain lying between the respective pairs of cross-link positions. The red arrow marks the region of greatest compliance in EF_OF_1, the dominant elastic buffer that is responsible for an elastic power transmission between F_O and F_1.

tional freedom of the bead in response to the magnetic field was limited. For both directions of rotation, the probability distribution showed 2 peaks. The respective forward directed peak was narrower and taller than the one where the enzyme had snapped back after being pressed to its forward limiting position. When the magnetic field was off, the bead fluctuated approximately around the middle position of its forced rotation. If, in some single molecules, this approximate symmetry was absent (dominating surface contacts?) the respective data were discarded. The reproducibility of the thermal fluctuations after switching off the magnetic field after a counterclockwise and a clockwise turn is demonstrated by the red and the blue histograms in Fig. 4*B Upper*. From the FWHM of these distributions, ≈7°, the torsional stiffness of the eccentric bearing was calculated to be 1,500 pNnm.

Summary and Discussion

Fig. 5 summarizes the data. It shows a section through the enzyme in gray and, in color, the cysteine pairs serving to establish a disulfide lock between rotor and stator. The total stiffness, κ_{total}, as detected when closing the respective disulfide bridge, is indicated in matching color at the horizontal bar. The partial stiffness of certain subsections of the enzyme is indicated at the vertical arrows. The bottom line is as follows: (*i*) The thin end of the rotor, i.e., the coiled-coil portion plus the C-terminal helix of subunit γ is of medium stiffness ($\kappa \cong 750$ pNnm); (*ii*) both the bulk of F_1, $(\alpha\beta)_3$, and the eccentric stator are very stiff ($\kappa \cong 1{,}500$ pNnm); (*iii*) only the enzyme portion between γ87C, subunit ε, and the **c**-ring is more compliant ($\kappa \cong 68$ pNnm); (*iv*) the most compliant domain is located between the sites where the respective power strokes in F_1 and F_O are generated (red arrow in Fig. 5), i.e., where good

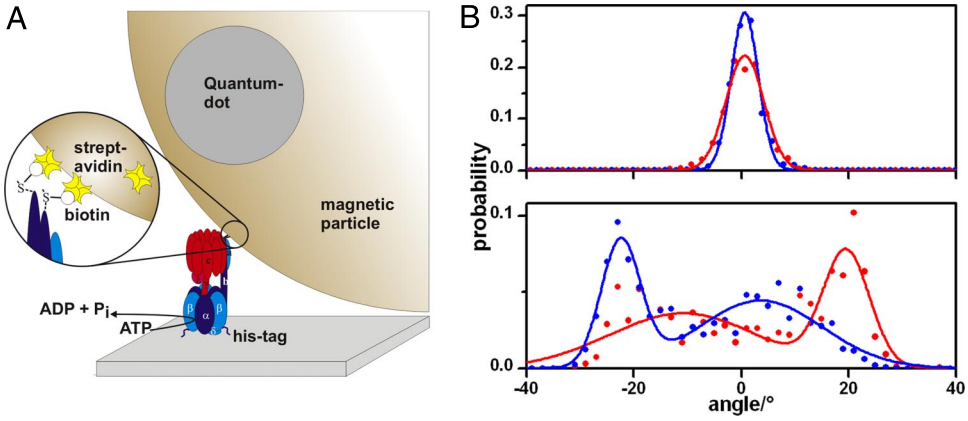

Fig. 4. Immobilized EF_OF_1 with a Q-dot-doped magnetic bead attached to the C-terminal end of both copies of subunit b (*A*) and histograms of rotary fluctuations (*B*) with the magnetic field off (*Upper*) and slowly (0.125 revolutions per second) rotating (*Lower*). The rotation was either clockwise (when viewed from the F_O side), shown in blue, or counterclockwise, shown in red. The fluctuations in the absence of the magnetic field (*Upper*) shown in blue and red, respectively, were observed subsequent to a previous clockwise and counterclockwise motion. The points are experimental, and the lines fits with a single Gaussian (*Upper*) and with 2 Gaussians each (*Lower*).

BIOPHYSICS

mechanical engineering would have placed it; and (*v*) if the DELSEED lever is free to undergo hinge motion, as during the ATP-waiting dwell, it contributes another rotary torsional compliance with a stiffness of ≈50 pNnm.

Hydrolysis of ATP by EF_OF_1 produces an average torque of 50 pNnm as determined from the curvature of a F_O-attached actin filament by the same single-molecule setup illustrated in Fig. 2*A* (4). If the holoenzyme operates in its native coupling membrane, and if it reaches thermodynamic equilibrium, then the forward torque generated by ionmotive force (by F_O) counterbalances the backward torque by ATP hydrolysis (by F_1), and the elastic element between them is maximally wound up. Taking the above-determined stiffness of the most-compliant domain of EF_OF_1 as 68 pNnm, it implies that the rotor is twisted by an angle of $\phi = M/\kappa = \frac{50}{68}$ or 42°, whereas the eccentric bearing is only negligibly twisted by <2°. This amounts to the storage of elastic energy of $U = M^2/2\kappa = 18$ pNnm or 11.1 kJ/mol.

How do these figures compare with those that have been hypothesized or indirectly inferred in previous studies? Simulations of the kinetic behavior of the enzyme taking the transient storage of elastic energy have led to gross estimates for the torsional stiffness of the elastic buffer, 60 pNnm (13) and 30 pNnm (14), respectively. A stored elastic energy (6 $k_BT \rightarrow 24.7$ pNnm $\rightarrow 14.9$ kJ/mol) has been calculated for the elastic hinge motion in subunit β (15). The former figures resulted from rather indirect kinetic or theoretical approaches. The experimentally observed smoothing of the discrete power strokes of F_1 after being transmitted to F_O has led to an estimate for stiffness in the order of 60 pNnm (4). The figures for the stiffness of the major elastic element between F_O and F_1 resulting from the present work, $\kappa \cong 68$ pNnm, and for the buffered elastic energy, $U \cong 11$ kJ/mol, are of the same magnitude as the former ones. However, the elastic buffer has now been experimentally attributed to a given domain, namely the bulky segment including the large, globular domains of subunits γ and ε plus the loops of the ring of subunit **c** to which they are attached.

Our results qualified the role of 3 enzyme domains that were tentatively discussed in this role: (*i*) The eccentric bearing was rather stiff (see Fig. 4*B*) [for the large binding strength of subunits δ and $\mathbf{b}_2$ to the hexagon of $(\alpha\beta)_3$ see refs. 22–24, and for a comprehensive review on $\mathbf{b}_2$ see ref. 21]. (*ii*) The elasticity of the hinge motion of the DELSEED region of subunit β has been previously emphasized in theoretical studies (15, 25). We have found that it matters during the turnover of the active enzyme, but it is not the main determinant of the elastic power transmission. (*iii*) When discussing the inner elasticity of F_OF_1, several groups (e.g., ref. 26) including our own have emphasized a role of the coiled coil plus the extended C terminus of subunit γ. Deletion studies (27, 28) have shown that this portion of the enzyme, extending from the counterpart on subunit γ of the DELSEED domain toward the supposed "hydrophobic bearing" (6), is dispensable for torque generation by F_1, although it is helpful for enzyme assembly and stability (27). Because it is (*i*) much less compliant than the main elastic buffer associated with the globular portions of γ and ε and (*ii*) mobile in its bearing (29, 30), the coiled-coil region of subunit γ cannot be claimed as the main elastic buffer.

That the main compliance is associated with the globular portions of γ and ε in contact with the **c**-ring is in line with the observation that these enzyme domains are not well-resolved in crystals of both F_1 (6) and F_OF_1 (11). Our data provide a basis for testing the predictive power of normal mode analysis (31) and molecular-dynamics simulations (31–36) of this particularly agile enzyme.

Because of the existence of an elastic buffer between the 2 stepping rotary motors in ATP synthase, any fine-tuning between the partial ion-transport events occurring in F_O and the partial chemical reactions (e.g., cleavage of certain hydrogen bonds) in F_1 is dispensable. The elastic power transmission explains why the enzyme can work by the same principles with different gears (3:10–15) in different organisms and why it operates robustly even in structurally modified (27, 28, 37–39) and in chimeric constructs with F_O and F_1 taken from different sources (40). The essential function of the elastic buffer is to provide this stepping rotary enzyme with high kinetic efficiency, in other words, with a high rate of turnover under load (3, 4).

Materials and Methods

Molecular Genetics. This work was carried out with 3 plasmids, namely pKH4, pSE1, and pKH7, and their derivatives. pKH4, the starting plasmid, had all wild-type cysteines substituted by alanines and carried a His_6 tag at the N terminus of subunit β (41). The plasmid pSE1, based on pKH4, carried a Strep-tagged C terminus in subunit **c** (16). The plasmid pKH7, based on pKH4, carried 1 extra cysteine, γK108C. The plasmid pSW3, based on pKH7, carried the cysteine pair βD380C/γA87C and is described in ref. 42. The pKH7-based plasmid pMM25, carrying the cysteine pair αE284C/γA270C, was a kind gift of M. Müller (University of Osnabrück, Osnabrück, Germany).

pSE1 was used as the starting plasmid for the mutations αE284C/γL276C, **a**I223C/**c**L72C, and βD380C/γA87C, resulting in the plasmids pGH14, pGH33, and pGH47, respectively. pBluescript II SK (+/−) subclones were generated by insertion of the following fragments of pSE1: KpnI/XhoI and KpnI/SacI for pGH14, BamHI/HindIII and BsrGI/PpuM for pGH33, and KpnI/SacI for γA87C in pGH47. Site-directed mutagenesis was carried out by PCR using the oligonucleotide 5′-CGCCAGGACGTTGTGCATTCCCGG-3′ and its complement 5′-CCGGGAATGCACAACGTCCTGGCG-3′ for αE284C, 5′-GCATTACTCAGGAATGCACCGAGATCGTCTCG-3′ and its complement 5′-CGAGACGATCTCGGTGCATTCCTGAGTAATGC-3′ for γL276C, 5′-CCGGTGAGCTGATTTTCTGTCTGATTGCTGGTCTGTTGC-3′ and its complement 5′-GCAACAGACCAGCAATCAGACAGAAAATCAGCTCACCGG-3′ for **a**I223C, 5′-CGCTGTAGGTCTGGGTTGCTACGTGATGTTCGCTGTC-3′ and its complement 5′-GACAGCGAACATCACGTAGCAACCCAGACCTACAGCG-3′ for **c**L72C, and 5′-CGACCGACCGTGGTTTGTGTGGTGGTTTGAAC-3′ and its complement 5′-GTTCAAACCACCACACAAACCACGGTCGGTCG-3 for γA87C (43). KpnI/XhoI, BsrGI/PpuM, and KpnI/SacI fragments of pSE1 were substituted with the corresponding fragments carrying the αE284C, **c**L72C, and γA87C mutations by standard restriction and ligation, resulting in plasmids pKG7, pGH39, and pGH46, respectively. The double mutants αE284C/γL276C, and **a**I223C/**c**L72C were then generated by exchanging the KpnI/SacI and BamHI/HindIII fragments of pKG7 and pGH39 with the corresponding mutated fragments of the pBluescript II SK (+/−) subclones by standard restriction and ligation, resulting in the plasmids pGH14, and pGH33, respectively. The plasmid pGH47 was obtained by exchanging XbaI/SacI fragment of pGH46 with the respective fragment of pSW3, carrying the mutation βD380C, by standard restriction and ligation. Successful cloning was checked by nucleotide sequencing.

A cysteine residue was added to the N terminus of the **b** subunit by site-directed mutagenesis by the following procedures. A 756-bp BsaHI fragment of pKH4 including the gene for subunit **c** and most of the gene for subunit **b** was cloned into pUC8 that had been cut with AccI to produce pSD300, with the insert in the reverse orientation relative to expression. Site-directed mutagenesis was carried out by PCR using pSD300 as the template with the mutagenic oligonucleotide 5′-CAGAAC*GTTAAC*TAAATAGAGGCATTGTGCT**GTGAATTGT**ATGAATCTTAACGCAACAATC-3′ and the M13 reverse primer. The mutagenic oligonucleotide included the HpaI site (italics) located upstream of the uncF start codon, and a 3-codon insertion (bold) at the start of uncF, retaining the natural GUG start codon. This insertion changed the N-terminal amino acid sequence encoded from MNLN to MNCMNLN. The PCR product was cut with HpaI and EcoRI and inserted into pSD300 that had been cut with the same enzymes to produce plasmid pSD303. After DNA sequencing, this plasmid was cut with PpuMI and BsrGI, and the 431-bp fragment was inserted into pKH4 that had been cut at unique sites with the same enzymes to produce plasmid pSD308.

Preparation of EF_1 and EF_OF_1. The preparation of EF_1, derived from the plasmids pSW3 and pMM25, followed the same procedures published previously (27, 42).

EF_OF_1, derived from the plasmids pGH14, pGH33, and pGH47, was prepared and purified via its Strep-tags as described in ref. 16.

EF_OF_1 based on pSD308, lacking the Strep-tag in **c**, was purified via its His tags as follows: Membrane protein was obtained as above, followed by centrifugation at 100,000 × *g* for 90 min. The supernatant was diluted with buffer A [20 mM Tris·HCl (pH 7.5), 50 mM KCl, 5 mM $MgCl_2$, 10% (vol/vol) glycerol, 20 mM imidazole] to 1% (wt/vol) *N*-octyl-L-D-glucopyranoside final concentration and applied (3 times) to an empty NAP5 column packed with 1 ml of Ni-NTA-Superflow. Wash was done with 5 ml of buffer A and then with the same buffer containing 150 mM imidazole. Glycerol (70%) was added to eluates before they were quick-frozen in liquid nitrogen and stored at −80°C before use.

Preparation of F-Actin. The preparation of F-actin followed the same procedures published previously (16).

Preparation of Magnetic Beads. Streptavidin-coated hyperparamagnetic beads (stock solution 10 mg/ml, diameter 1 μm; Roche) for experiments with EF_1 or $EFOF_1$ were diluted 10-fold with 50 mM Mops/KOH (pH 7.5), 50 mM KCl, and 5 mM $MgCl_2$ (buffer B) or 50 mM Mops/KOH (pH 7.5), 50 mM KCl, 5 mM $MgCl_2$, 0.5% (wt/vol) *N*-octyl-L-D-glucopyranoside, and 10% (vol/vol) glycerol (buffer C), respectively. The dilute suspension was centrifuged (16,000 $\times$ *g*, 4 °C, 3 min), and the pellet was resuspended in buffer B or buffer C. This washing procedure was repeated 3 times.

Immobilization of EF_1 and EF_OF_1. Similar procedures were used for immobilizing EF_1 and EF_OF_1. Samples were filled into flow cells consisting of 2 coverslips (bottom 26 $\times$ 76 mm^2; top 24 $\times$ 24 mm^2) separated by double-adhesive tape (Tesa). EF_OF_1 protein solutions were stepwise infused as described previously (16) by using buffer C in all steps. 50 μM–5 mM ATP was used in the last step. For ADP inhibition, 50 μl of 20 mM glucose, 0.2 mg/ml glucose oxidase, 50 μg/ml catalase (oxygen scavenger system, OSS), 0.5% 2-mercaptoethanol (2-me), 1 unit/μl hexokinase, and 5 mM ADP in buffer C were added after washing with 50 μl of buffer C.

The infusion order for EF_1 was as follows (50 μl per step, 4-min incubation, wash with buffer B before each step): (*i*) 0.8 μM Ni-NTA-horseradish peroxidase conjugate in buffer B; (*ii*) 10 mg/ml bovine serum albumin in buffer B; (*iii*) 5 μM EF_1 in buffer B; (*iv*) 0.2 mg/ml magnetic beads in buffer B (7-min incubation); (*v*) 2 pM Q-dots (stock 2 μM, dilution factor 1:1.000.000; Quantum Dot) in buffer B (7-min incubation); (*vi*) OSS, 0.5% 2-me, 20 mM DTT, and 5 mM ATP in buffer B. For pSD308-based EF_OF_1, the infusion followed the same instructions as for EF_1 (without 20 mM DTT in step *vi*), but replacing buffer B with buffer C.

For oxidization of both EF_OF_1 and EF_1, 50 μl of OSS, 0.2 mg/ml creatine kinase, 2.5 mM creatine phosphate, 1–2 mM Ellman's reagent, and 5 mM ATP in buffer C or buffer B were added after washing with 50 μl of buffer C or buffer B, respectively. For reducing of EF_1 after oxidization, 50 μl of OSS, 0.5% 2-me, 20 mM DTT, 10 mM $Na_2S_2O_4$, and 5 mM ATP in buffer B were added after washing with 50 μl of buffer B.

Video Microscopy. EF_1 and EF_OF_1 constructs were observed, and single-molecule rotation was recorded with an inverted fluorescence microscope as published (16). Fast bleaching of the fluorescently labeled actin filaments in the oxidized state was overcome by reducing the excitation intensity. Video data were captured with a Pinnacle DV500 Plus video card, and digitized with Adobe Premiere 6.0. A software program for evaluation of the obtained video sequences was written with Matlab 7.

Homology Modeling. Our model of EF_OF_1 was based on the structure as determined by Abrahams *et al.* [PDB ID Code 1bmf, (6)]. Modeling was carried out with the programs WhatIf (44) and O (45). The model coordinates are available from www.biologie.uni-osnabrueck.de/Biophysik/Engelbrecht/se/data/ef1/.

ACKNOWLEDGMENTS. We are very grateful for excellent technical assistance by Gaby Hikade and Yumin Bi (molecular biology) and Hella Kenneweg (single-molecule microscopy). This work was supported by Deutsche Forschungsgemeinschaft Grant SFB431/P1 (to S.E.), the European Union (W.J. and S.E.), the Volkswagen Foundation (W.J.), the Fonds der Chemie (W.J.), and the Canadian Institutes of Health Research (S.D.D.).

1. Junge W, Lill H, Engelbrecht S (1997) ATP synthase: An electrochemical transducer with rotatory mechanics. *Trends Biochem Sci* 22:420–423.
2. Wang HY, Oster G (1998) Energy transduction in the F_1 motor of ATP synthase. *Nature* 396:279–282.
3. Junge W, *et al.* (2001) Inter-subunit rotation and elastic power transmission in F_OF_1-ATPase. *FEBS Lett* 504:152–160.
4. Pänke O, Cherepanov DA, Gumbiowski K, Engelbrecht S, Junge W (2001) Viscoelastic dynamics of actin filaments coupled to rotary F-ATPase: Torque profile of the enzyme. *Biophys J* 81:1220–1233.
5. Jiang W, Hermolin J, Fillingame RH (2001) The preferred stoichiometry of c subunits in the rotary motor sector of *Escherichia coli* ATP synthase is 10. *Proc Natl Acad Sci USA* 98:4966–4971.
6. Abrahams JP, Leslie AGW, Lutter R, Walker JE (1994) The structure of F_1-ATPase from bovine heart mitochondria determined at 2.8 Å resolution. *Nature* 370:621–628.
7. Nishizaka T, *et al.* (2004) Chemomechanical coupling in F_1-ATPase revealed by simultaneous observation of nucleotide kinetics and rotation. *Nat Struct Mol Biol* 11:142–148.
8. Shimabukuro K, *et al.* (2003) Catalysis and rotation of F_1 motor: Cleavage of ATP at the catalytic site occurs in 1 ms before 40 degree substep rotation. *Proc Natl Acad Sci USA* 100:14731–14736.
9. Yasuda R, Noji H, Yoshida M, Kinosita K, Jr, Itoh H (2001) Resolution of distinct rotational substeps by submillisecond kinetic analysis of F_1-ATPase. *Nature* 410:898–904.
10. Pogoryelov D, *et al.* (2007) The C_{15}-ring of the *Spirulina platensis* F-ATP synthase: F_1/F_o symmetry mismatch is not obligatory. *EMBO Rep* 6:1040–1044.
11. Stock D, Leslie AG, Walker JE (1999) Molecular architecture of the rotary motor in ATP synthase. *Science* 286:1700–1705.
12. Junge W, Nelson N (2005) Nature's rotary electromotors. *Science* 308:642–644.
13. Cherepanov DA, Mulkidjanian A, Junge W (1999) Transient accumulation of elastic energy in proton translocating ATP synthase. *FEBS Lett* 449:1–6.
14. Pänke O, Rumberg B (1999) Kinetic modeling of rotary CF_0F_1-ATP synthase: Storage of elastic energy during energy transduction. *Biochim Biophys Acta* 1412:118–128.
15. Sun S, Chandler D, Dinner AR, Oster G (2003) Elastic energy storage in beta-sheets with application to F1-ATPase. *Eur Biophys J* 32:676–683.
16. Pänke O, Gumbiowski K, Junge W, Engelbrecht S (2000) F-ATPase: Specific observation of the rotating c subunit oligomer of EF_OEF_1. *FEBS Lett* 472:34–38.
17. Cherepanov DA, Junge W (2001) Viscoelastic dynamics of actin filaments coupled to rotary F-ATPase: Curvature as an indicator of the torque. *Biophys J* 81:1234–1244.
18. Tsunoda SP, *et al.* (2000) Observations of rotation within the F_OF_1-ATP synthase: Deciding between rotation of the F_oc subunit ring and artifact. *FEBS Lett* 470:244–248.
19. Del Rizzo PA, Bi Y, Dunn SD, Shilton BH (2002) The ''second stalk'' of *Escherichia coli* ATP synthase: Structure of the isolated dimerization domain. *Biochemistry* 41:6875–6884.
20. Revington M, Dunn SD, Shaw GS (2002) Folding and stability of the b subunit of the F(1)F(0) ATP synthase. *Protein Sci* 11:1227–1238.
21. Dunn SD, Revington M, Cipriano DJ, Shilton BH (2000) The b subunit of *Escherichia coli* ATP synthase. *J Bionenerg Biomembr* 32:347–355.
22. Häsler K, Pänke O, Junge W (1999) On the stator of rotary ATP synthase: the binding strength of subunit delta to $(\alpha\beta)_3$ as determined by fluorescence correlation spectroscopy. *Biochemistry* 38:13759–13765.
23. Weber J, Wilke-Mounts S, Nadanaciva S, Senior AE (2004) Quantitative determination of direct binding of b subunit to F_1 in *Escherichia coli* F_1F_0-ATP synthase. *J Biol Chem* 279:11253–11258.
24. Diez M, *et al.* (2004) Binding of the b-subunit in the ATP synthase from *Escherichia coli*. *Biochemistry* 43:1054–1064.
25. Ma J, *et al.* (2002) A dynamic analysis of the rotation mechanism for conformational change in F(1)-ATPase. *Structure (London)*10:921–931.
26. Menz RI, Walker JE, Leslie AG (2001) Structure of bovine mitochondrial F(1)-ATPase with nucleotide bound to all three catalytic sites: Implications for the mechanism of rotary catalysis. *Cell* 106:331–341.
27. Müller M, Pänke O, Junge W, Engelbrecht S (2002) F_1-ATPase: The C-terminal end of subunit γ is not required for ATP hydrolysis-driven rotation. *J Biol Chem* 277:23308–23313.
28. Hossain MD, *et al.* (2006) The rotor tip inside a bearing of a thermophilic F1-ATPase is dispensable for torque generation. *Biophys J* 90:4195–4203.
29. Muller M, *et al.* (2004) Rotary F1-ATPase. Is the C-terminus of subunit gamma fixed or mobile? *Eur J Biochem* 271:3914–3922.
30. Sabbert D, Engelbrecht S, Junge W (1996) Intersubunit rotation in active F-ATPase. *Nature* 381:623–625.
31. Cui Q, Li G, Ma J, Karplus M (2004) A normal mode analysis of structural plasticity in the biomolecular motor F(1)-ATPase. *J Mol Biol* 340:345–372.
32. Bockmann RA, Grubmuller H (2002) Nanoseconds molecular dynamics simulation of primary mechanical energy transfer steps in F1-ATP synthase. *Nat Struct Biol* 9:198–202.
33. Yang W, Gao YQ, Cui Q, Ma J, Karplus M (2003) The missing link between thermodynamics and structure in F1-ATPase. *Proc Natl Acad Sci USA* 100:874–879.
34. Dittrich M, Hayashi S, Schulten K (2003) On the mechanism of ATP hydrolysis in F1-ATPase. *Biophys J* 85:2253–2266.
35. Bockmann RA, Grubmuller H (2003) Conformational dynamics of the F1-ATPase beta-subunit: A molecular dynamics study. *Biophys J* 85:1482–1491.
36. Pu J, Karplus M (2008) How subunit coupling produces the gamma-subunit rotary motion in F1-ATPase. *Proc Natl Acad Sci USA* 105:1192–1197.
37. Cipriano DJ, Bi Y, Dunn SD (2002) Genetic fusions of globular proteins to the epsilon subunit of the *Escherichia coli* ATP synthase: Implications for in vivo rotational catalysis and epsilon subunit function. *J Biol Chem* 277:16782–16790.
38. Sorgen PL, Caviston TL, Perry RC, Cain BD (1998) Deletions in the second stalk of F_1F_0-ATP synthase in *Escherichia coli*. *J Biol Chem* 273:27873–27878.
39. Sorgen PL, Bubb MR, Cain BD (1999) Lengthening the second stalk of F(1)F(0) ATP synthase in *Escherichia coli*. *J Biol Chem* 274:36261–36266.
40. Kaim G, Dimroth P (1995) Formation of a functionally active sodium-translocating hybrid F_1F_0 ATPase in *Propionigenium modestum* by homologous recombination. *Eur J Biochem* 218:937–944.
41. Noji H, *et al.* (1999) Rotation of *Escherichia coli* F(1)-ATPase. *Biochem Biophys Res Comm* 260:597–599.
42. Gumbiowski K, *et al.* (2001) F-ATPase: forced full rotation of the rotor despite covalent cross-link with the stator. *J Biol Chem* 276:42287–42292.
43. Weiner MP, *et al.* (1994) Site-directed mutagenesis of double-stranded DNA by the polymerase chain reaction. *Gene* 151:119–123.
44. Vriend G (1990) WHAT IF: A molecular modeling and drug design program. *J Mol Graphics* 8:52–56, 29.
45. Jones TA, Zou JY, Cowan SW, Kjeldgaard M (1991) Improved methods for binding protein models in electron density maps and the location of errors in these models. *Acta Crystallogr A* 47:110–119.
46. Sielaff, H, Rennekamp, H, Engelbrecht, S, Junge, W (2008) Functional halt positions of rotary F_OF_1-ATPase correlated with crystal structures. *Biophys J* 95:4979–4987.